BIOCHEMISTRY
including biophysical chemistry & molecular biology

Article

pubs.acs.org/biochemistry

Role of Ion Valence in the Submillisecond Collapse and Folding of a Small RNA Domain

Suzette A. Pabit, Julie L. Sutton, Huimin Chen, and Lois Pollack*

School of Applied and Engineering Physics, Cornell University, Ithaca, New York 14853, United States

Supporting Information

ABSTRACT: Following the addition of ions to trigger folding, RNA molecules undergo a transition from rigid, extended states to a compact ensemble. Determining the time scale for this collapse provides important insights into electrostatic contributions to RNA folding; however, it can be challenging to isolate the effects of purely nonspecific collapse, e.g., relaxation due to backbone charge compensation, from the concurrent formation of some tertiary contacts. To solve this problem, we decoupled nonspecific collapse from tertiary folding using a single-point mutation to eliminate tertiary contacts in the small RNA subdomain known as tP5abc. Microfluidic mixing with microsecond time resolution and Förster resonance energy transfer detection provides insight into the ionic strength-dependent transition from extended to compact ensembles. Differences in reaction rates are detected when folding is initiated by monovalent or divalent ions, consistent with equilibrium measurements illustrating the enhanced screening of divalent ions relative to monovalent ions at the same ionic strength. Ion-driven collapse is fast, and a comparison of the collapse time of the wild-type and mutant tP5abc suggests that site binding of Mg^{2+} occurs on submillisecond time scales.

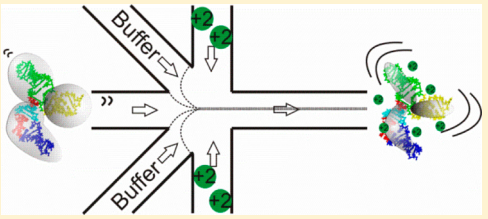

RNA plays important biological roles in translation, splicing, and enzymatic and catalytic reactions.[1] A recent focus on the role of RNA in the control of gene expression indicates that RNA molecules can be exploited for biotechnology applications.[2,3] Growing interest in the use of RNA aptamers and riboswitches as therapeutic and analytic agents[4] calls for a process of designing molecules on the basis of insights from RNA folding kinetic mechanisms.[5]

Structurally, RNA is a collection of short base-paired helices connected by non-base-paired regions that include loops, bulges, hinges, and junctions.[6,7] Because the RNA backbone carries a high negative charge, strong repulsive electrostatic forces must be overcome for the molecule to fold. RNA folding is induced in vitro by the addition of ions. Crystal structures reveal a small number of site-bound ions in some RNAs;[8] however, the majority of counterions form a diffuse cloud around the macromolecule.[9] In low-salt unfolded states, the helices repel and molecular conformations are extended. Following the addition of counterions to trigger folding, the backbone charge is more locally screened and the molecules relax to compact states. Recent equilibrium studies suggest that this "electrostatic relaxation" is anisotropic; the junctions direct folding by entraining helix motions along certain well-defined pathways.[10,11] Native contacts can then form when the two sides of a tertiary contact come into the proximity of each other. However, studies of short base-paired helices suggest that the negative duplex charge is not fully compensated on intramolecular length scales.[12] An outward electrostatic pressure opposes tight compaction in the absence of tertiary contacts, even at moderate to high ionic strengths. Thus, RNA folding is a balance between weakened, but non-negligible repulsive electrostatic forces and attractive forces, e.g., hydrogen bonding between the two sides of a tertiary contact. The primary goal of this study is to complement the increasing number of RNA folding and kinetic studies[13,14] by focusing on the process of collapse upon addition of charge-compensating ions. How does the rapid, initial collapse depend on the valence and concentration of counterions used to trigger it?

Previous small-angle X-ray scattering (SAXS) studies of the *Tetrahymena* ribozyme and selected mutants reveal a rapid compaction upon the addition of ions.[15] Concurrent time-resolved hydroxyl radical footprinting experiments show that the majority (but not all) of tertiary contacts in the molecule remain unformed within the time scale of rapid collapse. However, collapse occurred within the mixing dead times of those kinetic measurements, so only an upper limit for the collapse time (milliseconds) was obtained. More extensive time-resolved SAXS studies of the collapse and folding of the *Azoarcus* ribozyme[16] were conducted to focus on this initial rapid collapse. This group I intron displayed heterogeneous folding kinetics when folding was initiated by Mg^{2+}.[16] Some subpopulations collapse rapidly with tertiary contacts formed; others undergo nonspecific collapse before slower structural rearrangements can occur. Thus, the millisecond time scales reported for this system do not distinguish pure nonspecific collapse due to charge compensation from specific collapse. Other attempts to measure pure electrostatic collapse in simplified systems were obscured by the presence of a stiff

Received: December 14, 2012
Revised: February 8, 2013
Published: February 12, 2013

   dx.doi.org/10.1021/bi3016636 | *Biochemistry* 2013, 52, 1539−1546

hinge joining two helical domains that precluded relaxation to a compact ensemble.[17]

An experiment to measure the time scale of ion-mediated electrostatic collapse in RNA requires a clear delineation between nonspecific collapse (purely electrostatically driven) and specific collapse (containing native or non-native tertiary contacts). We accomplish this by choosing a molecule that collapses but is incapable of forming tertiary contacts, the A186U mutant of the tP5abc subdomain of the *Tetrahymena* ribozyme. In this well-characterized construct, mutation of a specific contact residue for Mg^{2+} binding[18] prevents secondary structure rearrangement, which is a prerequisite for the final steps of tertiary folding.[19] Nuclear magnetic resonance (NMR) studies have shown that the A186U mutant has an extended structure similar to that of wild-type tP5abc but does not undergo tertiary folding;[20] therefore, it is used as a control for unfolded tP5abc or the P4−P6 domain.[21−23] A recent publication focusing on the later folding steps of wild-type tP5abc speculates about the tight connection between secondary structure rearrangement and tertiary contact formation, suggesting that they occur concomitantly.[23] Use of the A186U mutation ensures that we probe only nonspecific collapse without the participation of tertiary contacts, allowing us to elucidate the nature of structures within the rapidly formed, compact ensemble.

Here, we describe the dependence of the earliest events in RNA folding on ion type, valence, and concentration, using the A186U mutation in tP5abc RNA to monitor the formation of the collapsed state. Fluorescence correlation spectroscopy (FCS) measurements verify that this construct collapses to a compact state in high-salt solutions. To establish the electrostatic contributions of different ions in facilitating collapse, we quantify the strength of electrostatic interactions using second virial coefficients (A_2) of short RNA duplexes determined by SAXS. Because theoretical studies suggest that ion-driven nonspecific collapse in RNA should occur on submillisecond time scales,[24,25] we use a microfluidic mixer with microsecond time resolution[26] combined with Förster resonance energy transfer (FRET) detection in a confocal microscope to measure the kinetics of RNA collapse caused by a rapid increase in salt concentration. Between solutions with the same counterion valence, we measure collapse times that decrease as the ionic strength increases, reflecting the increasing entropy of the collapsed state with ionic strength as suggested by equilibrium measurements.[27] Near physiological monovalent ionic strengths, the initial nonspecific collapse is fast and occurs with a time comparable to the dead time of our rapid mixing microfluidic device (≈200 μs). When Mg^{2+} is used to initiate folding, collapse times are faster in the wild type than in the mutant, suggesting that site binding of Mg^{2+} occurs within the first millisecond of folding, faster than previously implied using techniques with slower time resolution.[28,29] Our data suggest that specific contact formation accelerates the earliest steps of folding and "directs" folding along specific pathways.

MATERIALS AND METHODS

Materials. RNA molecules were synthesized, desalted, and purified by Dharmacon RNAi Technologies (Lafayette, CO). The sequence of the 25 bp double-stranded RNA used for second virial coefficient measurements is GCA UCU GGG CUA UAA AAG GGC GUCG as in previous studies.[30] We used the truncated P5abc (tP5abc) construct and its A186U mutant described by Wu and Tinoco[19] for fluorescence correlation spectroscopy (FCS) and rapid mixing experiments. We have added a uracil to the 5′ end to prevent interactions between the donor and the nearby G-C base pair. The 5′ end was labeled with the donor fluorophore (fluorescein), while the A171 nucleotide in the P5c stem−loop structure was labeled with the acceptor fluorophore (Dy547, with spectral characteristics similar to those of Cy3). The positions of the labels were chosen such that a change in Förster resonance energy transfer (FRET) between the extended and collapsed states of tP5abc can be measured. The tP5abc RNA molecules were stored in 50 mM K^+-MOPS buffer (pH 7) with 0.1 mM EDTA. Prior to measurements, they were annealed in 20 mM K^+-MOPS buffer (pH 7) with 8 mM EDTA at 50 °C for 5 min and then slowly cooled to room temperature. The molecules were buffer-exchanged to 20 mM K^+-MOPS buffer (pH 7) for all experiments, and different salt solutions were added to change ion conditions. Monovalent and divalent ion solutions were prepared from chloride salts unless stated otherwise. All chemicals were purchased from Sigma (St. Louis, MO). The rotational motion of the dye labels was investigated using fluorescence anisotropy measurements. Results are described in the Supporting Information and shown in Figure S1 of the Supporting Information.

Second Virial Coefficient Measurements. The strength of intermolecular interactions between 25 bp RNA duplexes was assessed by extracting the second virial coefficient (A_2) from SAXS profiles measured as a function of RNA concentration at varying cation valence and salt concentrations. A_2 is a measure of the interaction potential between short RNA helices in solution and takes into account the contributions from excluded volume, electrostatic repulsion, and interhelical attraction.[12,30−32] The SAXS experiments for measuring A_2 were conducted at the Cornell High Energy Synchrotron Source (CHESS) and are described extensively in previous publications.[12,30]

Equilibrium Fluorescence Measurements. FCS was used to measure the changes in the diffusion times of tP5abc under different ionic conditions. Molecules in the collapsed state are more compact and diffuse faster than molecules in extended and unfolded configurations. The standard confocal setup described by Chen et al.[33] used a 488 nm laser for fluorescein excitation. Data processing and fitting were performed with Origin (Microcal, Northampton, MA). Equilibrium FRET was calculated from fluorescence spectra taken with a Cary Eclipse fluorescence spectrophotometer (Varian Inc.). The effective efficiency of energy transfer (E_{FRET}) was calculated as $A/(A + D)$, where A and D are the peak intensities of the acceptor and donor emission, respectively.

Rapid Mixing To Measure RNA Collapse. We used a microfluidic mixer to rapidly change the ionic conditions of the tP5abc RNA.[26,34] The mixer uses hydrodynamic focusing[35,36] to facilitate fast diffusion of ions into the RNA sample. The experimental conditions are described in the Supporting Information with a schematic of the device shown in Figure S2 of the Supporting Information. The mixing dead time for K^+ and Rb^+ ions was 140 μs, and that for Mg^{2+} and Sr^{2+} ions was 235 μs. Additional details of the manufacture, characterization, and use of the mixing device were published in previous work.[26] Devices were fabricated at the Cornell NanoScale Science and Technology Facility (CNF).

RESULTS

Dependence of Charge Screening on Ion Valence for RNA Duplexes. To characterize how ions affect charge screening interactions between RNA helices, we used SAXS to measure A_2 between 25 bp RNA duplexes as a function of ion type and ionic strength. End effect contributions to A_2 are minimal when duplex lengths exceed ~25 bp,[32] allowing us to focus on how ions affect screening lengths measured from the cylindrical axis of the double helix. We find that the charge screening efficiency depends on ion valence but not ion type (Figure 1A). Measured values of A_2 in Na^+, K^+, and Rb^+ agree within experimental error, while values of A_2 in Mg^{2+} and Sr^{2+} are indistinguishable. Furthermore, these results are consistent with previous experiments showing that divalent ions provide more efficient charge screening than monovalent ions at the same ionic strengths.[9,27,37−41] A cartoon illustrating the ionic strength dependence of charge screening efficiency is shown in Figure 1B. Because A_2 can be expressed in units of volume,[31] we associate an electrostatic excluded volume with each duplex at every ionic strength, denoted by the shaded balloon in the figure. At the lowest ionic strength, where A_2 has its largest value and intermolecular repulsion dominates, this excluded volume is large. As the ionic strength increases and the duplex negative charge is more efficiently screened, both A_2 and the excluded volume decrease, allowing the helices to approach each other more closely. At even higher ionic strengths, A_2 becomes negative and interhelical attraction consistent with end-to-end stacking is observed.[12,30] In the cartoon representation (Figure 1B) for $A_2 < 0$, the electrostatic excluded volume is small enough to allow other interaction forces to take effect.

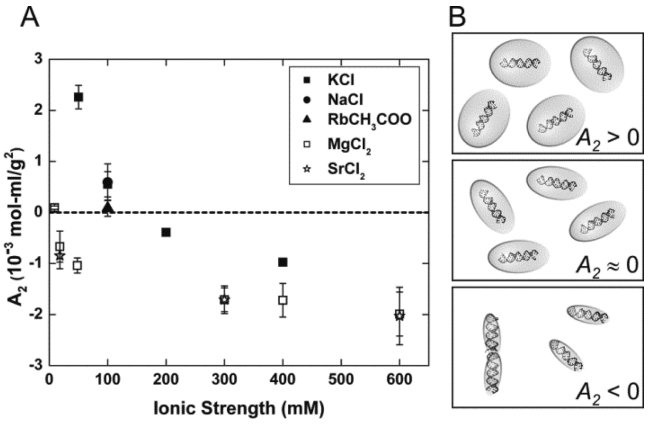

Figure 1. We use the second virial coefficient (A_2) to quantify the ionic strength-dependent intermolecular interaction potential of 25 bp RNA helices. Positive values of A_2 denote intermolecular repulsion, while negative values of A_2 can reflect duplex association via end-to-end stacking.[12,30] (A) A_2 measurements of 25 bp RNA duplexes obtained from SAXS data. As the ionic strength increases, the interhelix repulsion decreases because of stronger screening of RNA charges by counterions. Values of A_2 in solutions with monovalent cations [KCl (■), NaCl (●), and $RbCH_3COO$ (▲)] are indistinguishable, as are those with divalent cations [$MgCl_2$ (□) and $SrCl_2$ (☆)]. However, for a given ionic strength, divalent ions are more effective in screening the charges than monovalent ions. (B) Cartoon illustrating the electrostatic excluded volume at increasing ionic strengths. When $A_2 > 0$, large repulsive forces between helices are represented by large electrostatic excluded volumes. When $A_2 \approx 0$, the RNA−RNA interactions are negligible. $A_2 < 0$ represents RNA association via end-to-end stacking.[30]

The A_2 measurements shown in Figure 1A allow a quantitative comparison of the screening effectiveness of different ionic solutions. Clearly, ionic strength alone is insufficient to explain the RNA charge screening efficiency of ions with different valences, but comparison between ions of the same valence reveals similar electrostatic effects.

Equilibrium Fluorescence Measurements of tP5abc. The tP5abc RNA consists of three helices (P5a−P5c) connected at a junction by single-stranded regions as shown in Figure 2A.[19] At low salt concentrations, the three helices of tP5abc are arranged in an extended state (Figure 2B). Increasing the bulk salt concentration reduces the repulsive forces among the three helices; therefore, we expect the RNA to collapse to more compact conformations as salt is added. Because a more extended molecule has a larger hydrodynamic radius and diffuses more slowly, compaction is signaled by a decrease in the diffusion time of the RNA.

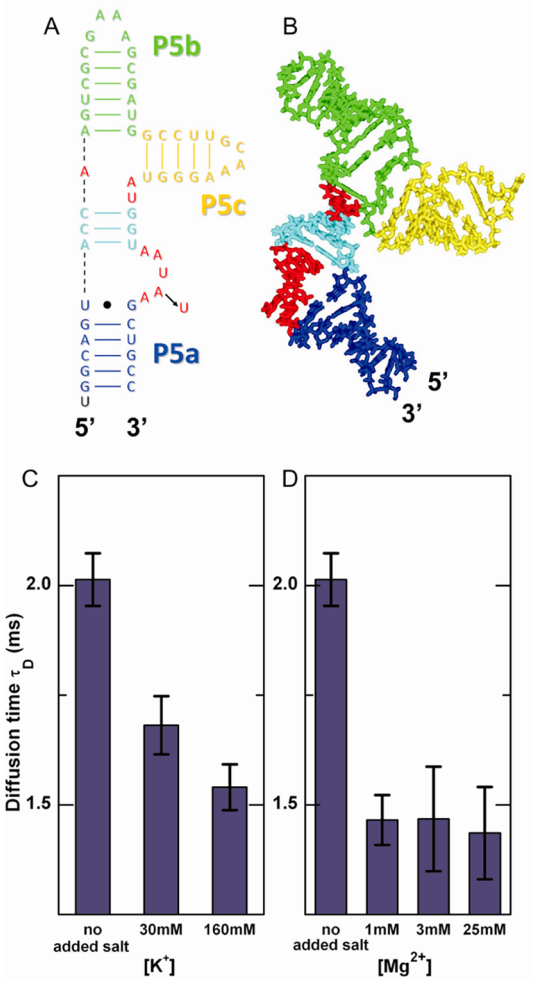

Figure 2. tP5abc collapses with an increasing ionic strength. (A) Extended state secondary structure of tP5abc.[19] The A186U mutation is denoted with an arrow. (B) tP5abc extended state conformation in solution,[20] shown with the same color scheme as in panel A. (C and D) Diffusion times of the A186U mutant obtained from FCS measurements in K^+ and Mg^{2+}, respectively. A dramatic decrease in τ_D is observed upon the addition of salt, demonstrating tP5abc compaction with the increase in bulk counterion concentration.

We used FCS to monitor the A186U mutant, which has the same extended state secondary structure as the wild type but

dx.doi.org/10.1021/bi3016636 | Biochemistry 2013, 52, 1539−1546

does not form tertiary contacts and thus does not fold to the native state.[18,19] A single diffusion constant (τ_D) and two exponential time constants (τ_A and τ_B) were needed to adequately fit the FCS data. The presence of only one diffusion component indicates the absence of conformational states with substantially different diffusion times and thus different hydrodynamic radii. In addition to the characteristic diffusion time, two fast characteristic fluctuation time components are required to accurately fit the FCS data. We tentatively attribute these time scales to a combination of internal molecular motions leading to fluctuations in FRET and dye photophysics. At increased ionic strengths, FCS data report a dramatic decrease in τ_D (Figure 2C,D). Because τ_D is proportional to the hydrodynamic radius of the molecule, the different values measured in the initial (low salt concentration, 9 mM K^+) buffer and the final solution [containing an additional 30 or 160 mM K^+ (Figure 2C) or 1, 3, or 25 mM Mg^{2+} (Figure 2D)] indicate collapse to a compact state. FCS measurements of wild-type tP5abc show the same trends and diffusion times comparable to those of the mutant (Figure S3 of the Supporting Information); however, because of its lack of sensitivity, FCS cannot further distinguish the folded (wild type) from the collapsed (mutant) states. Figure S4 of the Supporting Information shows the diffusion times of the mutant in solutions containing different ionic species. Similar to second virial measurements, we see no significant dependence of diffusion time on ion type.

Equilibrium FRET measurements were also performed under different ionic conditions. In our case, FRET cannot be used as a quantitative probe of the size of the molecule because fluorescence anisotropy measurements show that the internally labeled acceptor dye was not freely rotating in solution (see the Supporting Information for details). Figure S5 of the Supporting Information shows the effective equilibrium E_{FRET} of the tP5abc wild type and mutant under different ionic conditions. We see no significant dependence of E_{FRET} on monovalent ion type, but there is a slight difference between Mg^{2+} and Sr^{2+} ions. Because FCS and A_2 measurements cannot detect this difference, it is possibly due to a change in the local dye environment during divalent ion-aided collapse. Nonetheless, a normalized change in FRET efficiency still signals a conformational change upon addition of ions and can be used to compare time scales of collapse for each ion type. Additional equilibrium fluorescence control experiments are discussed in the Supporting Information and shown in Figure S6 of the Supporting Information.

Measurement of Collapse Times under Different Ionic Conditions. The equilibrium measurements discussed above suggest that tP5abc and its mutant, held in a low-salt concentration solution, become compact following the addition of ions. To gain insight into the energy landscape of collapse, we measured the collapse time (τ_c) of the A186U nonfolding mutant under several different experimental conditions using microfluidic mixing.[26] Mixing of ions is facilitated by diffusion after hydrodynamic focusing[35,36] as described in the Supporting Information. Initially, RNA is equilibrated in a low-salt buffer (9 mM K^+), where FCS indicates that it populates extended states. To focus on the collapse transition, we measured how the effective E_{FRET} changed over time when the A186U mutant was rapidly mixed with buffers under different ionic conditions. The signal was normalized by the measured E_{FRET} from a control experiment in which the RNA was mixed with the same low-salt buffer as in its initial state. The resulting normalized E_{FRET} versus time was fit to a single-exponential decay with a constant offset to extract τ_c. Figure 3 shows representative, normalized kinetic traces at different concentrations of added divalent ions.

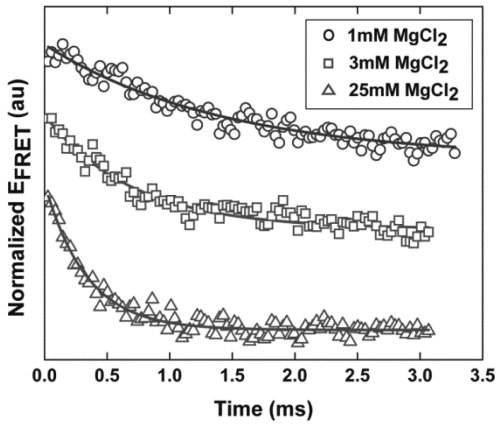

Figure 3. Typical normalized kinetic traces of the tP5abc A186U mutant after it had been mixed with different Mg^{2+} concentrations. Solid lines represent single-exponential fits to the data. Offsets have been added to the traces to separate them.

The time scale for collapse (Figure 4) displays a marked decrease with an increasing ionic strength. At the highest ionic strengths measured, the collapse time is comparable to the dead times of the mixing instrument (indicated by cross-hatched regions in Figure 4). To test its importance on ion type, we measured the collapse time scale in solutions containing 30 mM K^+ or 30 mM Rb^+ and 1 mM Mg^{2+} or 1 mM Sr^{2+}. These lower ionic strengths enhanced our sensitivity to differences by

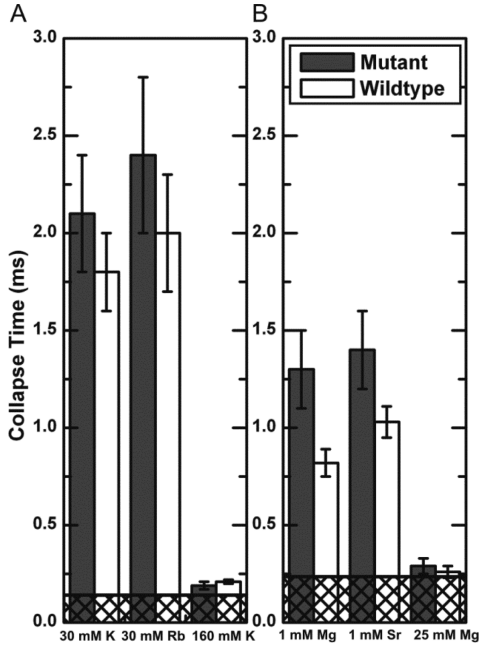

Figure 4. Collapse times of tP5abc rapidly mixed with (A) monovalent and (B) divalent ions. Collapse of the mutant does not depend on ion type (30 mM K^+ and Rb^+ or 1 mM Mg^{2+} and Sr^{2+}). The wild type collapses faster than the mutant in 1 mM Mg^{2+}, suggesting early binding of Mg^{2+} to the specific binding site. Cross-hatched regions represent the mixer dead times [140 (A) and 235 μs (B)].

dx.doi.org/10.1021/bi3016636 | Biochemistry 2013, 52, 1539−1546

increasing the separation between mixing and collapse time scales.

Results for the nonfolding A186U mutant show no significant dependence of collapse time on ion type. Thus, for both monovalent and divalent ions, nonspecific collapse depends on the valence and concentration, but not the identity, of the ion. Similarly, as we expect, there are no differences between the collapse times of the wild type and the mutant in monovalent salt solutions (Figure 4A).

Previous studies using hydroxyl radical footprinting have found folding times for the isolated P5abc domain to be slow, on the time scale of tens to hundreds of milliseconds.[17,42] Other studies used stopped-flow fluorescence to measure a folding time of 240 ms for wild-type tP5abc in 1 mM Mg^{2+} and show that secondary structure rearrangement is rate-limiting for the tertiary folding of wild -type tP5abc.[19,20,23] Because our rapid mixing results give us faster time resolution than the previous measurements cited, we are observing a transition of the extended wild-type molecule to a compact set of states in which tertiary contacts and secondary structure rearrangement have not yet occurred.

To discern the importance of specific Mg^{2+} binding to rapid compaction, we compare the collapse time of the mutant with that of wild-type tP5abc. At 1 mM Mg^{2+}, the collapse time of the wild type is 0.82 ± 0.07 ms compared with a time of 1.3 ± 0.2 ms for the mutant (Figure 4B). The small but significant difference between collapse times of the wild type and the nonfolding mutant suggests that something other than electrostatic screening stabilizes the collapsed state of the wild type. We also investigated the effect of ion type in the collapse of wild-type tP5abc and measured a time of 1.03 ± 0.08 ms in 1 mM Sr^{2+}, which is slower than the collapse in 1 mM Mg^{2+} (0.82 ± 0.07 ms). The difference in collapse time of the wild type due to different divalent ions is small and just outside the error bars. While it is only in the wild type where we can confidently distinguish between collapse times because of ions of different types, we note the same general trend for both the mutant and wild type.

DISCUSSION

Impact of Ion Valence and Type on Collapse Times. Measurements of second virial coefficients of model systems detect minimal differences in intermolecular interactions based on ion type. At a given ionic strength, K^+, Rb^+, and Na^+ have identical second virial coefficients, as do Mg^{2+} and Sr^{2+} (Figure 1A). We also tested the effectiveness of various ions in inducing the collapse transition in the A186U mutant. No ion type effects were observed in nonspecific collapse: τ_c does not distinguish 30 mM K^+ from 30 mM Rb^+, or 1 mM Mg^{2+} from 1 mM Sr^{2+}. However, these effects do not scale across solutions of different valence ions. The FCS, A_2, and previous persistence length measurements[38] confirm that charge screening of the RNA phosphate backbone is more efficient in divalent than monovalent ions. This is, in fact, what we observe in the kinetic measurements (see Figure 4).

From Debye–Hückel (DH) arguments alone, we expect nonspecific electrostatic effects to be determined solely by ionic strength. However, the anomalous behavior of divalent relative to monovalent ions is a frequent theme in studies of nucleic acid electrostatics.[22,27,37,38,43] Consistent with literature reports, in the kinetic experiments reported here, mixing with divalent ions leads to a shorter collapse time than mixing with monovalent ions at a given ionic strength. Although some studies may suggest that spatially correlated counterions can lead to enhanced screening of polyelectrolytes, these effects seem to be more evident when the counterion valence is >2.[44,45] For the case of divalent ions, some insight can be gleaned from recent MD simulations of ions around RNA.[46] Notably, simulation results agree with DH models with large distances from the RNA: screening is a function of ionic strength at distances from the central axis of the molecule of >16 Å. However, to achieve this agreement requires adjustment of the surface charge density near the RNA surface. Close to the surface, both nucleic acid topologies and the distinctive features of counterions (and co-ions) are important. Mean field models are inapplicable because they cannot account for atomic detail ab initio. Our measurements suggest that the surface potential is smaller in the presence of divalent ions, because of their tighter localization and the larger degree of charge compensation. As a result, there is simply less charge to screen at larger distances where the mean field theory can be applied. In terms of the model shown in Figure 1B, the electrostatic excluded volume is smaller for divalent than monovalent ions at a given ionic strength, because the "near charge" on the duplex is more completely neutralized. Thus, differences result from the ions that are closest to the RNA surface.

The Ionic Strength Dependence of Collapse Reflects Increasing Conformational Entropy in the Collapsed Ensemble. Our results can be placed into the context of recent reports suggesting that tP5abc folding is a sequential process with at least two barriers.[23] While the previous work focused on understanding the transition from the collapsed intermediate to the folded state,[23] our use of a submillisecond mixing device and a nonfolding mutant allowed us to focus on the formation of the collapsed state from an extended conformation. For a given ion valence, we find that collapse times decrease with an increasing salt concentration (Figures 3 and 4). To explain our results, we propose a simple model based on the concept of electrostatic excluded volume, derived from the second virial coefficients (see Results and Figure 1B). Within this model, the ionic strength dependence of τ_c is readily explained. With no added salt, the A186U mutant exists in an extended (or unfolded) state (U) due to the large electrostatic excluded volume of its three helices. With the addition of charge-compensating ions, the electrostatic excluded volume decreases as illustrated in Figure 5A, and more conformations are available to the molecule. The more flexible, collapsed collection of states (I) have increased conformational entropy relative to that of U, as suggested by Bai et al.[27] In the absence of tertiary contacts, there are minimal changes to the enthalpy, so the free energy decreases with respect to the extended state. Therefore, population of the collapsed state(s) is more favorable at increased ionic strengths, and the kinetic transition time τ_c decreases. It is interesting to note a recent report discussing other favorable entropic effects of tertiary folding as a function of increasing Mg^{2+} concentration.[47] Clearly, the role of thermodynamic contributions in ion-dependent RNA folding is still an open question and should be subject to further investigations. Future directions should involve temperature-dependent kinetic experiments with microsecond time resolution to examine the Arrhenius-type dependence of ion concentration.

Site-Bound Mg^{2+} Ions. To determine the effect of specific interaction on the initial stages of RNA collapse, we compared the collapse time of mutant and wild-type tP5abc in 1 mM Mg^{2+} and 1 mM Sr^{2+}. The crystal structure of the *Tetrahymena*

dx.doi.org/10.1021/bi3016636 | *Biochemistry* 2013, 52, 1539–1546

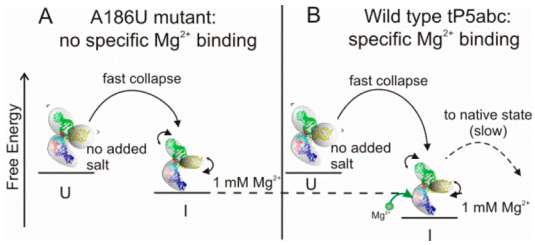

Figure 5. Possible schematic of the early stages of tP5abc collapse. (A) With no added salt, the A186U mutant exists in an extended (or unfolded) state (U) because of the large electrostatic excluded volume of its three helices. When rapidly mixed with ions, the molecule collapses to a compact intermediate state (I). The increase in ion concentration reduces the electrostatic excluded volume, allowing the molecule to become more flexible. This change increases its conformational entropy and reduces its free energy, which all lead to faster collapse times. (B) The same arguments as in panel A apply to wild-type tP5abc; however, specific binding of Mg^{2+} ions reduces the enthalpy of the collapsed state, which can manifest as a faster collapse time as observed in the mixing experiments. Once specific binding has occurred, the wild type can proceed to fold to its native state, although this step is slow because of the large free energy barrier of secondary structure rearrangement.

thermophila ribozyme's full P4−P6 domain shows five specific binding sites for Mg^{2+} ions within P5abc.[18] The A186U mutation disrupts one of these sites and prevents secondary structure rearrangement.[19] It is possible that the altered secondary structure is necessary for full coordination of the remaining bound Mg^{2+} ions; thus, this single mutation may disrupt all site binding. We speculate that the shorter collapse time in 1 mM Mg^{2+} reflects a more stable compact intermediate state of the wild type relative to that of the mutant (Figure 5B). We attribute the reduced free energy of the collapsed state of the wild type to the lower enthalpy contributed by binding of at least one Mg^{2+} ion. Thus, we suggest that Mg^{2+} binding occurs prior to either tertiary contact formation or secondary structure rearrangement, because these are known to occur more slowly.[17,23,42] Recent results of Koculi et al. showed that the slow step of wild-type tP5abc folding does not require binding of additional Mg^{2+} ions to the RNA.[23] This also suggests that Mg^{2+} binds early in the folding process. The submillisecond time scale measured here is much faster than previously suggested for Mg^{2+} binding;[28,29] however, those studies had only millisecond time resolution.

Our measurements indicate that the wild type collapses faster in 1 mM Mg^{2+} than in 1 mM Sr^{2+}. Evidence that Sr^{2+} cannot occupy the Mg^{2+} binding sites of P5abc[48] supports our proposal that the faster collapse of the wild type in Mg^{2+} is caused by bound ions. We note that while the difference in the collapse times of the wild-type RNA due to 1 mM Mg^{2+} and Sr^{2+} ions is just outside the error bars, the same trend (albeit statistically insignificant) can also be discerned in the mutant. An alternate explanation for this observation may be found in previous theoretical work that suggests that the presence of smaller ions (like Mg^{2+}) in the ion atmosphere increase the stability of the collapsed ensemble relative to larger ions with the same valence (Sr^{2+}).[49] However, the size of diffuse ions alone is not sufficient to account for the small difference in collapse time scales observed between the wild type and the mutant in the presence of 1 mM Sr^{2+}, where no specific binding occurs. Experimental techniques that specifically probe binding of Mg^{2+} and Sr^{2+} ions are needed to fully understand the contribution of Sr^{2+} ions in tertiary folding.

A Model of tP5abc Collapse and Folding. Taken together, and in the context of other folding measurements on the same molecule, our data present a unified picture of how this small domain acquires tertiary structure. In the initial, low-salt state, the molecule possesses the secondary structure that minimizes its free energy. Following the addition of ions to weaken the electrostatic repulsion between helices, the molecule favors more compact conformations. Mixing experiments indicate that formation of this collapsed ensemble occurs on the submillecond time scales predicted by theoretical studies of nonspecific collapse of RNA.[24,25] In the wild-type molecule, our results suggest that interactions of the Mg^{2+} ion with specific nucleotides in the A-rich bulge are concurrent with the rapid collapse. It is interesting to speculate that the early binding of Mg^{2+} may be the cause of the energetically expensive shift in secondary structure that distinguishes nonspecifically collapsed from folded states. The bound Mg^{2+} ion coordinated to A186 also interacts specifically with nucleotides in the nearby strands of the P5c stem−loop structure (Figure 2A). This interaction, coupled with dynamic fluctuations of the non-Watson−Crick base pairs near the three-helix junction, may assist with the secondary structure shift measured in fully folded tP5abc. The A186U mutation disrupts the binding of this Mg^{2+} ion, and the barrier for rearrangement can never be overcome. The very large barrier associated with the folding transition may account for the wide separation in time of the collapse and folding transitions and allows their separate study. Interestingly, the proposed Mg^{2+} binding site in the VS ribozyme is also near the sequence where a secondary structure shift occurs,[50] hinting that the binding of Mg^{2+} may facilitate energetically expensive shifts in RNA secondary structure.

■ CONCLUSIONS

We used a number of different experimental techniques (equilibrium SAXS and FCS, rapid mixing with FRET detection) to relate the electrostatic properties of isolated RNA elements (double-stranded and non-base-paired regions) to the kinetic folding behavior of a small RNA domain. We find that nonspecific electrostatic interactions are important in determining the conformational space accessed by a compact molecule that lacks tertiary contacts, which in turn is related to the time scale for collapse. Divalent ions are very effective in electrostatic screening and generate rapid collapse rates comparable to those of monovalent ions at much higher ionic strengths. We propose that divalent ions are more effective than monovalent ions in charge screening because of their tighter localization around the RNA helix. Comparison of the collapse times of the wild type and A186U mutant of tP5abc RNA in divalent ions shows that folding RNA sequences collapse faster than their nonfolding mutants, supporting the concept that specific interactions lead to the increased efficiency of RNA collapse. We suggest that specific binding of Mg^{2+} ions can occur even during the initial collapse and bias the reaction. Our results highlight the differing roles of counterions in RNA folding kinetics and may aid the design and use of synthetic RNA for biotechnology applications.

■ ASSOCIATED CONTENT

Supporting Information

Discussion of fluorescence anisotropy measurements, discussion of equilibrium FRET, experimental details of the

microfluidic mixer, diffusion coefficients of salt solutions used in mixing experiments (Table S1), plot of fluorescence anisotropy results (Figure S1), schematic of the mixing device (Figure S2), additional FCS results (Figures S3 and S4), and equilibrium FRET results (Figure S5). This material is available free of charge via the Internet at http://pubs.acs.org.

AUTHOR INFORMATION

Corresponding Author

*Telephone: (607) 255-8695. Fax: (607) 255-7658. E-mail: lp26@cornell.edu.

Author Contributions

S.A.P. and J.L.S. contributed equally to this work.

Funding

This work was supported by National Institutes of Health Grant R01-GM085062. CHESS is supported by the National Science Foundation (NSF) and the National Institutes of Health/National Institute of General Medical Sciences via NSF Grant DMR-0936384. CNF, a member of the National Nanotechnology Infrastructure Network, is supported by the National Science Foundation (ECS-0335765).

Notes

The authors declare no competing financial interest.

ACKNOWLEDGMENTS

We acknowledge useful discussions with Steve Meisburger, Ron Elber, and Serdal Kirmizialtin and experimental assistance from Ken Finkelstein, Arthur Woll, Watt Webb, Warren Zipfel, Avtar Singh, Christopher Jones, Hye Yoon Park, David Rigie, and Natalie Paquette. We thank Ignacio Tinoco for sharing extended state structures.

ABBREVIATIONS

FRET, Förster resonance energy transfer; FCS, fluorescence correlation spectroscopy; SAXS, small-angle X-ray scattering; A_2, second virial coefficient.

REFERENCES

(1) Doudna, J. A., and Cech, T. R. (2002) The chemical repertoire of natural ribozymes. *Nature 418*, 222−228.

(2) Eddy, S. R. (2001) Non-coding RNA genes and the modern RNA world. *Nat. Rev. Genet. 2*, 919−929.

(3) Mattick, J. S., and Makunin, I. V. (2006) Non-coding RNA. *Hum. Mol. Genet. 15* (Special Issue 1), R17−R29.

(4) Link, K. H., and Breaker, R. R. (2009) Engineering ligand-responsive gene-control elements: Lessons learned from natural riboswitches. *Gene Ther. 16*, 1189−1201.

(5) Westhof, E., Masquida, B., and Jaeger, L. (1996) RNA tectonics: Towards RNA design. *Folding Des. 1*, R78−R88.

(6) Butcher, S. E., and Pyle, A. M. (2011) The molecular interactions that stabilize RNA tertiary structure: RNA motifs, patterns, and networks. *Acc. Chem. Res. 44*, 1302−1311.

(7) Cruz, J. A., and Westhof, E. (2009) The dynamic landscapes of RNA architecture. *Cell 136*, 604−609.

(8) Bowman, J. C., Lenz, T. K., Hud, N. V., and Williams, L. D. (2012) Cations in charge: Magnesium ions in RNA folding and catalysis. *Curr. Opin. Struct. Biol. 22*, 262−272.

(9) Draper, D. E. (2004) A guide to ions and RNA structure. *RNA 10*, 335−343.

(10) Chu, V. B., Lipfert, J., Bai, Y., Pande, V. S., Doniach, S., and Herschlag, D. (2009) Do conformational biases of simple helical junctions influence RNA folding stability and specificity? *RNA 15*, 2195−2205.

(11) Bailor, M. H., Sun, X., and Al-Hashimi, H. M. (2010) Topology links RNA secondary structure with global conformation, dynamics, and adaptation. *Science 327*, 202−206.

(12) Li, L., Pabit, S. A., Lamb, J. S., Park, H. Y., and Pollack, L. (2008) Closing the lid on DNA end-to-end stacking interactions. *Appl. Phys. Lett. 92*, 223901−2239013.

(13) Al-Hashimi, H. M., and Walter, N. G. (2008) RNA dynamics: It is about time. *Curr. Opin. Struct. Biol. 18*, 321−329.

(14) Woodson, S. A. (2010) Compact intermediates in RNA folding. *Annu. Rev. Biophys. 39*, 61−77.

(15) Kwok, L. W., Shcherbakova, I., Lamb, J. S., Park, H. Y., Andresen, K., Smith, H., Brenowitz, M., and Pollack, L. (2006) Concordant exploration of the kinetics of RNA folding from global and local perspectives. *J. Mol. Biol. 355*, 282−293.

(16) Roh, J. H., Guo, L., Kilburn, J. D., Briber, R. M., Irving, T., and Woodson, S. A. (2010) Multistage collapse of a bacterial ribozyme observed by time-resolved small-angle X-ray scattering. *J. Am. Chem. Soc. 132*, 10148−10154.

(17) Schlatterer, J. C., Kwok, L. W., Lamb, J. S., Park, H. Y., Andresen, K., Brenowitz, M., and Pollack, L. (2008) Hinge stiffness is a barrier to RNA folding. *J. Mol. Biol. 379*, 859−870.

(18) Cate, J. H., Hanna, R. L., and Doudna, J. A. (1997) A magnesium ion core at the heart of a ribozyme domain. *Nat. Struct. Biol. 4*, 553−558.

(19) Wu, M., and Tinoco, I., Jr. (1998) RNA folding causes secondary structure rearrangement. *Proc. Natl. Acad. Sci. U.S.A. 95*, 11555−11560.

(20) Zheng, M., Wu, M., and Tinoco, I., Jr. (2001) Formation of a GNRA tetraloop in P5abc can disrupt an interdomain interaction in the *Tetrahymena* group I ribozyme. *Proc. Natl. Acad. Sci. U.S.A. 98*, 3695−3700.

(21) Silverman, S. K., Zheng, M., Wu, M., Tinoco, I., Jr., and Clech, T. R. (1999) Quantifying the energetic interplay of RNA tertiary and secondary structure interactions. *RNA 5*, 1665−1674.

(22) Greenfeld, M., Solomatin, S. V., and Herschlag, D. (2011) Removal of covalent heterogeneity reveals simple folding behavior for P4-P6 RNA. *J. Biol. Chem. 286*, 19872−19879.

(23) Koculi, E., Cho, S. S., Desai, R., Thirumalai, D., and Woodson, S. A. (2012) Folding path of P5abc RNA involves direct coupling of secondary and tertiary structures. *Nucleic Acids Res. 40*, 8011−8020.

(24) Lee, N., and Thirumalai, D. (2000) Dynamics of collapse of flexible polyampholytes. *J. Chem. Phys. 113*, 5126−5129.

(25) Thirumalai, D., Lee, N., Woodson, S., and Klimov, D. (2001) Early events in RNA folding. *Annu. Rev. Phys. Chem. 52*, 751−762.

(26) Park, H. Y., Qiu, X., Rhoades, E., Korlach, J., Kwok, L. W., Zipfel, W. R., Webb, W. W., and Pollack, L. (2006) Achieving uniform mixing in a microfluidic device: Hydrodynamic focusing prior to mixing. *Anal. Chem. 78*, 4465−4473.

(27) Bai, Y., Chu, V. B., Lipfert, J., Pande, V. S., Herschlag, D., and Doniach, S. (2008) Critical assessment of nucleic acid electrostatics via experimental and computational investigation of an unfolded state ensemble. *J. Am. Chem. Soc. 130*, 12334−12341.

(28) Silverman, S. K., and Cech, T. R. (2001) An early transition state for folding of the P4-P6 RNA domain. *RNA 7*, 161−166.

(29) Kim, H. D., Nienhaus, G. U., Ha, T., Orr, J. W., Williamson, J. R., and Chu, S. (2002) Mg^{2+}-dependent conformational change of RNA studied by fluorescence correlation and FRET on immobilized single molecules. *Proc. Natl. Acad. Sci. U.S.A. 99*, 4284−4289.

(30) Pabit, S. A., Qiu, X., Lamb, J. S., Li, L., Meisburger, S. P., and Pollack, L. (2009) Both helix topology and counterion distribution contribute to the more effective charge screening in dsRNA compared with dsDNA. *Nucleic Acids Res. 37*, 3887−3896.

(31) Bonnete, F., and Vivares, D. (2002) Interest of the normalized second virial coefficient and interaction potentials for crystallizing large macromolecules. *Acta Crystallogr. D58*, 1571−1575.

(32) Nicolai, T., and Mandel, M. (1989) The ionic strength dependence of the second virial coefficient of low molar mass DNA fragments in aqueous solutions. *Macromolecules 22*, 438−444.

(33) Chen, H., Rhoades, E., Butler, J. S., Loh, S. N., and Webb, W. W. (2007) Dynamics of equilibrium structural fluctuations of apomyoglobin measured by fluorescence correlation spectroscopy. *Proc. Natl. Acad. Sci. U.S.A. 104*, 10459−10464.
(34) Park, H. Y., Kim, S. A., Korlach, J., Rhoades, E., Kwok, L. W., Zipfel, W. R., Waxham, M. N., Webb, W. W., and Pollack, L. (2008) Conformational changes of calmodulin upon Ca^{2+} binding studied with a microfluidic mixer. *Proc. Natl. Acad. Sci. U.S.A. 105*, 542−547.
(35) Knight, J. B., Vishwanath, A., Brody, J. P., and Austin, R. H. (1998) Hydrodynamic Focusing on a Silicon Chip: Mixing Nanoliters in Microseconds. *Phys. Rev. Lett. 80*, 3863−3866.
(36) Pollack, L., Tate, M. W., Darnton, N. C., Knight, J. B., Gruner, S. M., Eaton, W. A., and Austin, R. H. (1999) Compactness of the denatured state of a fast-folding protein measured by submillisecond small-angle X-ray scattering. *Proc. Natl. Acad. Sci. U.S.A. 96*, 10115−10117.
(37) Qiu, X., Andresen, K., Kwok, L. W., Lamb, J. S., Park, H. Y., and Pollack, L. (2007) Inter-DNA attraction mediated by divalent counterions. *Phys. Rev. Lett. 99*, 038104.
(38) Chen, H., Meisburger, S. P., Pabit, S. A., Sutton, J. L., Webb, W. W., and Pollack, L. (2012) Ionic strength-dependent persistence lengths of single-stranded RNA and DNA. *Proc. Natl. Acad. Sci. U.S.A. 109*, 799−804.
(39) Woodson, S. A. (2005) Metal ions and RNA folding: A highly charged topic with a dynamic future. *Curr. Opin. Chem. Biol. 9*, 104−109.
(40) Chu, V. B., Bai, Y., Lipfert, J., Herschlag, D., and Doniach, S. (2008) A repulsive field: Advances in the electrostatics of the ion atmosphere. *Curr. Opin. Chem. Biol. 12*, 619−625.
(41) Lipfert, J., Sim, A. Y., Herschlag, D., and Doniach, S. (2010) Dissecting electrostatic screening, specific ion binding, and ligand binding in an energetic model for glycine riboswitch folding. *RNA 16*, 708−719.
(42) Deras, M. L., Brenowitz, M., Ralston, C. Y., Chance, M. R., and Woodson, S. A. (2000) Folding mechanism of the *Tetrahymena* ribozyme P4-P6 domain. *Biochemistry 39*, 10975−10985.
(43) McIntosh, D. B., and Saleh, O. A. (2011) Salt Species-Dependent Electrostatic Effects on ssDNA Elasticity. *Macromolecules 44*, 2328−2333.
(44) Ha, B., and Thirumalai, D. (2003) Bending Rigidity of Stiff Polyelectrolyte Chains: A Single Chain and a Bundle of Multichains. *Macromolecules 36*, 9658−9666.
(45) Andresen, K., Qiu, X., Pabit, S. A., Lamb, J. S., Park, H. Y., Kwok, L. W., and Pollack, L. (2008) Mono- and trivalent ions around DNA: A small-angle scattering study of competition and interactions. *Biophys. J. 95*, 287−295.
(46) Kirmizialtin, S., and Elber, R. (2010) Computational exploration of mobile ion distributions around RNA duplex. *J. Phys. Chem. B 114*, 8207−8220.
(47) Fiore, J. L., Holmstrom, E. D., and Nesbitt, D. J. (2012) Entropic origin of Mg^{2+}-facilitated RNA folding. *Proc. Natl. Acad. Sci. U.S.A. 109*, 2902−2907.
(48) Travers, K. J., Boyd, N., and Herschlag, D. (2007) Low specificity of metal ion binding in the metal ion core of a folded RNA. *RNA 13*, 1205−1213.
(49) Koculi, E., Hyeon, C., Thirumalai, D., and Woodson, S. A. (2007) Charge density of divalent metal cations determines RNA stability. *J. Am. Chem. Soc. 129*, 2676−2682.
(50) Andersen, A. A., and Collins, R. A. (2000) Rearrangement of a stable RNA secondary structure during VS ribozyme catalysis. *Mol. Cell 5*, 469−478.